1.7

APPLICATION OF AEROSONDES TO HIGH-RESOLUTION OBSERVATIONS OF SEA SURFACE TEMPERATURE OVER BARROW CANYON

Jun Inoue* and Judith A. Curry

School of Earth and Atmospheric Sciences, Georgia Institute of Technology, Atlanta, GA

1. INTRODUCTION

During September 2002, sea ice extent in the Arctic Ocean reached its lowest levels recorded since 1978 (Serreze et al. 2003). During this period, the ice reduction was not uniform over the Arctic Ocean, with substantial reduction observed in the Beaufort Sea. In general such reductions have been attributed to ice divergence and rapid melt promoted by the persistent low pressure and high temperatures over the summertime Arctic Ocean. However, an important contributor to melting can also be the condition of the upper-ocean water masses (e.g., Shimada et al. 2001).

Warm temperature in the Beaufort Sea typically arrives from northward flow from the Bering Strait to the Chukchi Sea (Aagaard et al. 1985; Overland and Roach 1987; Coachman and Aagaard 1988). During summer and early fall, warm and fresh Alaskan coastal waters from Eastern Bering Sea generally arrive at Point Barrow and pass through Barrow Canyon into the Arctic Ocean (Aagaard and Roach 1990). Therefore, the Barrow Canyon has been considered as a conduit of mass, heat, and momentum at the intersection of the broad Chukchi self, the narrow Beaufort shelf, and deep Arctic Ocean.

However, there is some evidence that SST and local currents in the vicinity of the Barrow Canyon may be changed by relatively colder water induced by coastal upwelling. Using an acoustic Doppler current profiler (ADCP) and a conductivity, temperature, and depth instrument (CTD), Johnson (1989) showed that the upwelling colder water was moving upcanyon (i.e., southwestward flow) induced by northeasterly wind. This reversal event occurs from 2 to 10 day's duration (Weingartner et al. 1998). Münchow and Carmack (1997) also pointed out that locally upwelling favorable winds which are along the western coast of Alaska, raise the Arctic halocline ventilated within Barrow Canyon adjacent to the coast. However, the weak coupling between Barrow Canyon flow and the local meteorology was also suggested because the major flow variations are principally part of large-scale oceanic phenomena, rather than being locally wind-driven (Aagaard and Roach 1990). Weingartner et al. (1998) showed that the yearly averaged winds were southward, while the mean currents were northward.

While observations obtained from moorings and ADCP have provided useful information about the vertical structure of the flow, such methods require a ship for deployment and the number of deployments is very limited. With regard to the surface characteristic flows, satellite data has proven to be useful (D'asaro 1988; Liu et al. 1994). However, space and time resolution of observations is limited using these observing systems.

The Aerosonde (Holland et al. 1992), a small robotic aircraft, provides a new capability for improving the space / time resolution of observations of the ice/ocean surface. The Aerosonde has a wing span of 9 m and weighs approximately 15 kg. Since 2000, the Aerosonde flies with a mean speed of about 25 m s^{-1} and is highly maneuverable. The small size of the Aerosonde allows it to be extremely fuel efficient so that flight durations can easily exceed 20 hours. Iridium satellite communications are vital to successfully exploiting the long range/long

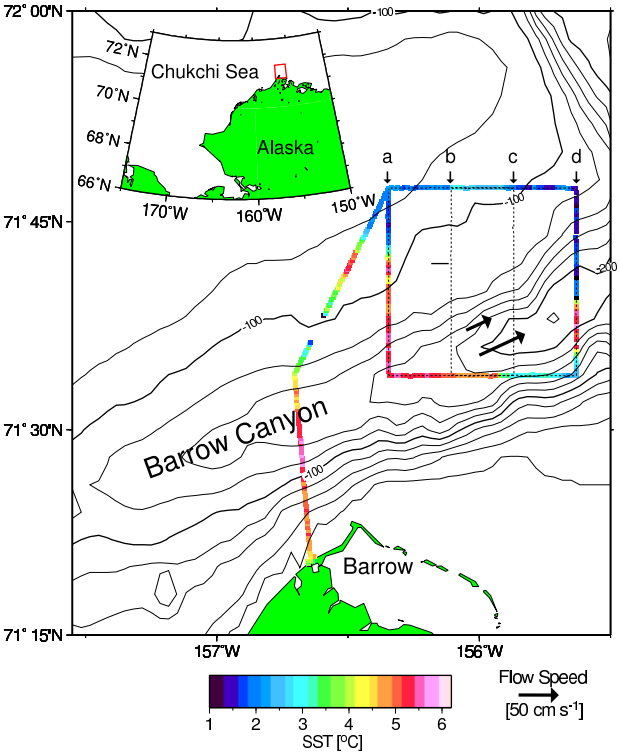

Figure 1: Map of the study area at the northwestern tip of Alaska. Observed SSTs during the box 1 flight (2200 UTC 19 Sep. – 0200UTC 20 Sep. 2002) are presented by colors. Contours represent bottom topography with the interval of 20 m. The labels (a, b, c, and d) indicate the different longitude to be used for making the time-latitude cross-sections in Figure 3. Thick black vectors denote the estimated flow speed in Figure 4.

* *Corresponding author address*: Jun Inoue, School of Earth and Atmospheric Sciences, Georgia Institute of Technology, Atlanta, GA 30332-0340, USA; e-mail: jun.inoue@eas.gatech.edu

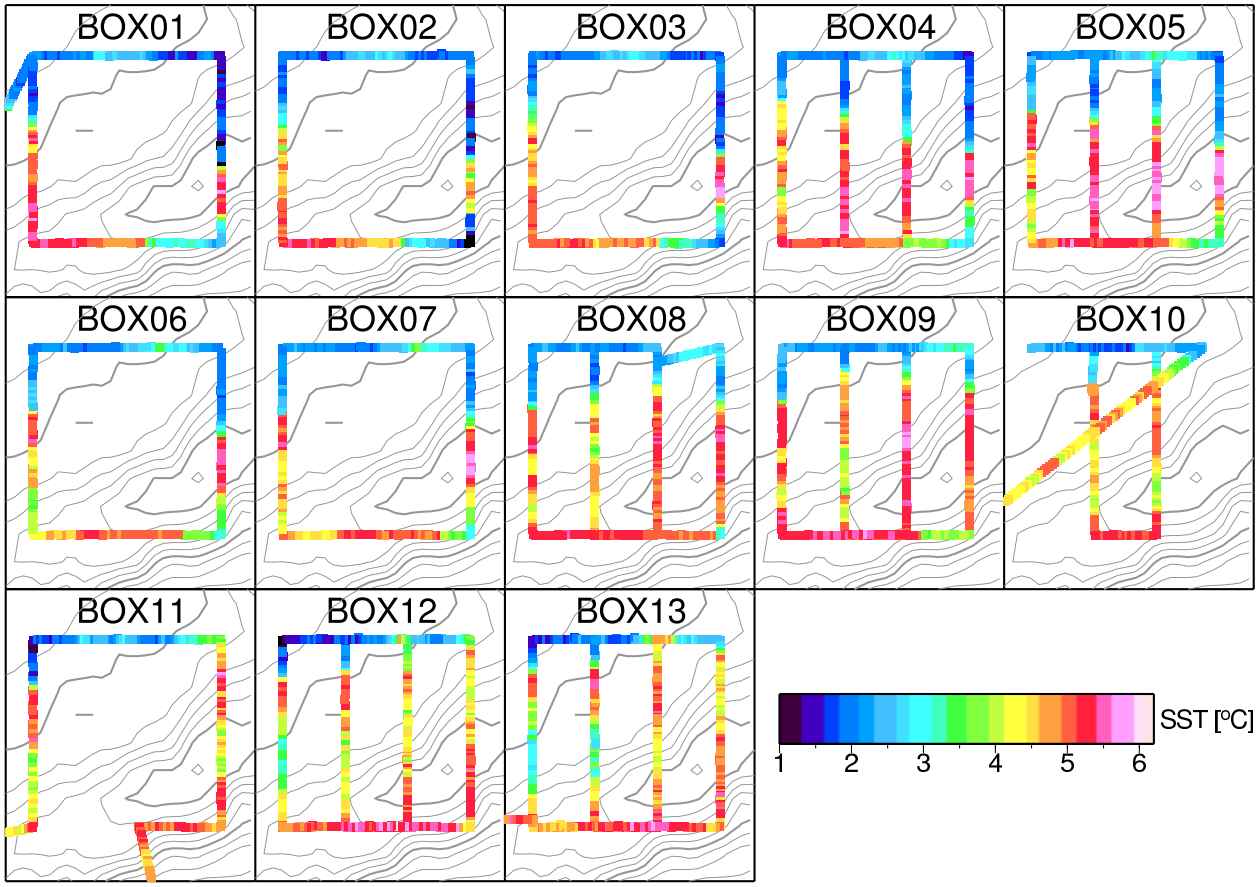

Figure 2: Horizontal distribution of the sea surface temperature for each box flight. Contours represent bottom topography as same in Figure 1.

endurance capabilities of the Aerosonde aircraft (nearly 3000 km). It has an altitude range of between 100 and 7000 m. Of relevance to this study, an Infrared Pyrometer (Heitronics Model: KT-11) is installed on the bottom of the Aerosonde fuselage to observe the sea surface temperature. Aerosondes have been making observations in the Beaufort/Chukchi Seas, based from Barrow, Alaska, since 2000 (Holland et al. 2001; Curry et al. 2004).

During September in 2002, Aerosondes took continuous observations of SST over the Barrow Canyon for a period of 27 hours on 20−21 September 2002. Two Aerosondes were launched at 2230 UTC 19 September and at 1850 UTC 20 September 2002, flying 17 and 10 hours, respectively. The flight pattern consisted of a box pattern with 25-km legs (Figure 1), in the vicinity of 71.7 °N, 156.0 °W. The Aerosonde altitude was maintained below cloud base between 150 and 250 m during the box patterns. This paper describes and interprets these observations.

2. OBSERVATIONS

During the Aerosonde operations, a high pressure system was passing over the observational area. The wind direction significantly changed from NE to SSE during the first half of the observational period, and SSE wind prevailed in the latter half of the flight period. Although the air temperature at Barrow decreased during the night-time (0500−1600 UTC), the temperature difference between the daytime and night-time was small ($\sim$ 1 K) due to the Arctic stratus clouds, suggesting that the local time change in the SST by surface cooling is small.

During these flights, a total of 13 box patterns were flown. A large box pattern was flown with 25×25 km (Boxes 1, 2, 3, 6, 7, and 11). Smaller boxes were flown within the larger boxes, including 25×8.3 km (Boxes 4, 5, 8, 9, 10, 12, and 13). It takes 1.5−2 hours to complete each box-pattern flight. Figure 2 shows the horizontal distribution of the SST for each box flight. The SST ranges from 1 to 6 °C, and the sharp SST front (3 K temperature difference) is located over the northwestern shelf of Barrow Canyon. This front appears to move northward; in particular, the motion at the most eastern side between the boxes 6−9 is significant. At the southwestern side of the box, relatively cold water (around 4 °C) appears to intrude (boxes 4−9), and this cold water is dominant towards the end of the period of observation (boxes 12−13). According to the horizontal distribution of SST prior to box 1 (Figure 1), this cold water was located in the region WSW of the box area, suggesting that the surface flow is northeastward (i.e., along the canyon).

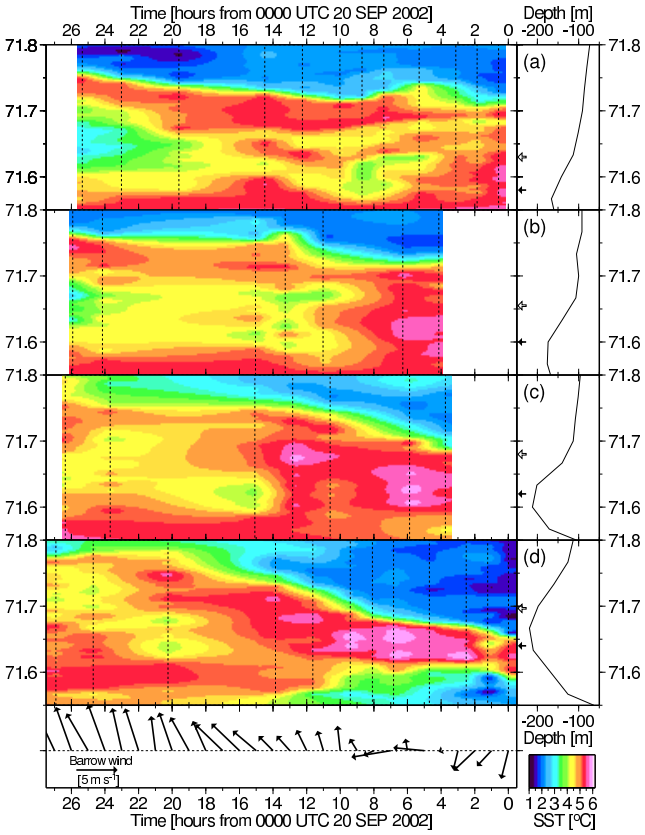

Figure 3: Time-latitude cross-sections of the SST by interpolating the observed SST on each longitude. Dotted lines indicate the time of the observation. The label of each cross-section (a, b, c, and d) corresponds to the label shown in Figure 1. The bottom topography along each section is also shown in the right panel. Black and white arrows in each panel show the latitude to calculate the time lag correlation coefficients over the axis of the canyon and northern slope, respectively. Lower panel indicates the time series of wind vector at Barrow. Time axis is the opposite of general one.

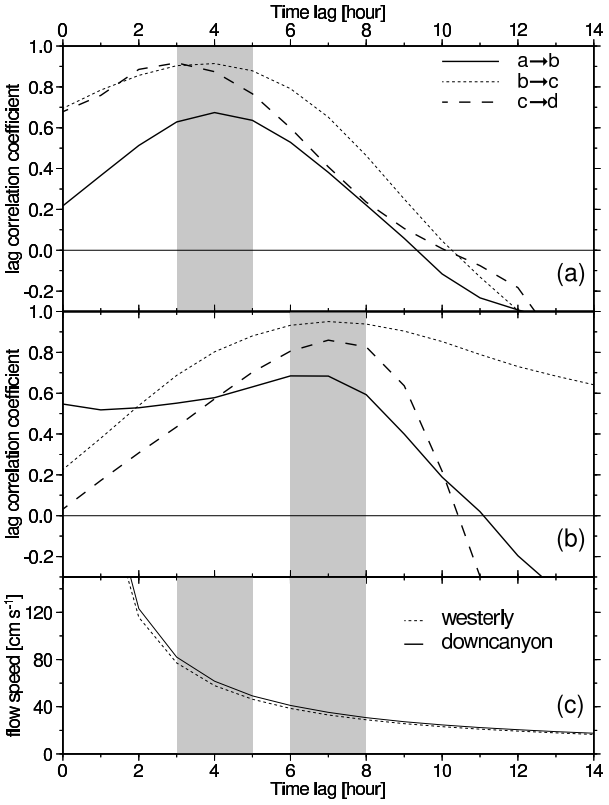

Figure 4: Lag correlation coefficients (a) at the axis of the canyon, and (b) at the northern slope of the canyon. (c) Estimated flow speed of westerly component (dotted line) and along-canyon component (thick line) as a function of time lag. Downcanyon component is calculated using an angle of 20 °T from the true east.

To investigate the surface flow in detail, time-latitude cross-sections of the SST were constructed using each north-south leg from each box pattern (Figure 3). We used 12 legs from the outer boxes (i.e., legs-a and -d denoted in Figure 1), and 7 legs from the inner boxes (i.e., legs-b and -c denoted in Figure 1). By focusing on the warmest water mass (exceeding 5 °C) near the axis of the canyon (at 0000 UTC and 71.58 °N in Figure 3a), we notice that the warm water mass moves along the canyon. This same feature can be seen in the relatively cold water mass which appears at 0800 UTC and 71.58 °N in the leg-a. These results suggest that along-canyon flow dominates over the Barrow Canyon (i.e., downcanyon flow). On the other hand, along the northern slope of the axis of the canyon, the flow speed seems to be relatively slow. For example, the warm water mass at 0000 UTC and 71.61 °N in the leg-a moved to the leg-b at 0600 UTC and 71.62 °N and to the leg-c at 1300 UTC and 71.68 °N. The intrusion of the cold water mass at 1900 UTC and 71.65 °N in leg-a also reached leg-b after 6 hours.

To estimate the surface flow speed over the axis of the canyon and the northern slope, the lag correlation coefficient of the observed SST was calculated using the hourly SST data which was interpolated linearly for each leg. Figure 4a shows the lag correlation coefficients between legs-a and -b (thick line), between legs-b and -c (dotted line), and between legs-c and -d (thick dashed line) at the specific latitude denoted by black arrows in Figure 3, respectively. Each latitude of the leg corresponds to the location of the axis of the canyon. The highest correlations were obtained at 3–5 hours' lag. Considering the distance between the adjacent legs (8.3 km), the westerly current component can be estimated to be 0.45–0.8 m s^{-1} (dotted line in Figure 4c). At the northern slope (denoted by white arrows in Figure 3), the time lag of the highest correlation increased (6–8 hours; Figure 4b), suggesting the slower flow speed (0.3–0.4 m s^{-1}; dotted line in Figure 4c). Assuming that the surface flow is closely aligned with the canyon axis, the components of the downcanyon flow can be also estimated (thick line in Figure 4) which have almost same as the westerly component due to the small angle of the direction of the canyon axis (about 20 °T from the true east). Horizontal distributions of the estimated flow pattern are depicted by vectors in Figure 1, suggesting the existence of a strong sheared flow into the Arctic Ocean through Barrow Canyon.

3. DISCUSSION

Over the 25 km square region investigated here centered on the Barrow Canyon, substantial variability in SST was observed, ranging from 1 to 6 °C. The time series of the SST observations were used to infer that the flow through Barrow Canyon has a strongly sheared flow into the Arctic Ocean. Although our estimation of the flow speed is not based on direct measurements, our estimated value agrees generally with previous observations. Using moorings, Aagaard and Roach (1990) and Weingartner et al. (1998) measured the currents near the bottom and over the shoreward flank of the canyon which were generally downcanyon (northeastward) to be about 0.2 m s^{-1} on the average with maximum speeds of $\sim$ 1.0 m s^{-1}. Münchow and Carmack (1997) observed the surface current by the ADCP in September 1993, and showed that a northward flowing jet which transports the Bering summer water into the Arctic Ocean exceeds 0.7 m s^{-1} through Barrow Canyon. This observed downcanyon flow was well reproduced by using a numerical model (Signorini et al. 1997).

During our observations, the wind direction changed from NNE to SSE (bottom panel in Figure 3). NNE wind (i.e., upwelling favorable winds) occurred continuously for more than 12 hours prior to our observation. Therefore, we may have observed the upwelling colder water near the eastern side of the canyon early in the observational period. However, according to the SST distribution just north from Barrow (Figure 1), the warm water occupied most of the shoreward flank of the canyon, suggesting that the colder water did not exist homogeneously along the canyon and the flow through the canyon is strongly temporal/spatial dependent. Therefore, the wind effect on the flow pattern is presumably weak in this situation.

In conclusion, the high temporal and spatial resolution of the Aerosonde observations has contributed to improved understanding of the scales of variability of ocean temperature and circulation in the coastal regions of the Arctic Ocean. Because of the platform capabilities and inexpensive cost, the Aerosonde has the potential to be a very useful platform in studying mesoscale ocean features, particularly if the Aerosonde observations can be coordinated with moorings and other in situ observation.

ACKNOWLEDGMENTS

This work was done under NSF grant number OPP-9910297 and DOE ARM program. We would like to thank DOE ARM for providing accommodations and internet access. Thanks are given to D. Ramey and M. Irinaga for providing logistics support under BASC. Special thanks are also afforded to the Aerosonde crews and CU participants whose tireless efforts have made the Aerosonde a success in the harsh Arctic environment.

REFERENCES

Aagaard, K., A. T. Roach, and J. D. Schumacher, 1985: On the wind-driven variability of the flow through Bering Strait, *J. Geophys. Res.*, **90**, 7213–7221.

Aagaard, K., and A. T. Roach, 1990: Arctic ocean-shelf exchange: Measurements in Barrow Cnyon, *J. Geophys. Res.*, **95**, 18,163–18,175.

Coachman, L. K., and K. Aagaard, 1988: Transports through Bering Strait: Annual and interannual variability, *J. Geophys. Res.*, **93**, 15,535–15,539.

Curry, J. A., J. M. Maslanik, G. J. Holland, and J. O. Pinto, 2004: Applications of Aerosondes in the Arctic, *Bull. Amer. Meteor. Soc.* (submitted).

D'asaro, E., 1988: Generation of submesoscale vortices: A new mechanism, *J. Geophys. Res.*, **93**, 6685–6693.

Holland, G. J., T. McGeer, and H. Youngren, 1992: Autonomous Aerosondes for economical atmospheric soundings anywhere on the globe, *Bull. Amer. Meteor. Soc.*, **73**, 1987-1998.

Holland, G. J., P. J. Webster, J. A. Curry, G. Tyrell, D. Gauntlett, G. Brett, J. Becker, R. Hoag, and W. Vaglienti, 2001: The Aerosonde robotic aircraft: A new paradigm for environmental observations, *Bull. Amer. Meteor. Soc.*, **82**, 889–901.

Johnson, W. R., 1989: Current response to wind in the Chukchi Sea: A regional coastal upwelling event, *J. Geophys. Res.*, **94**, 2057–2064.

Liu, A. K., C. Y. Peng, and T. J. Weingartner, 1994: Ocean-ice interaction in the marginal ice zone using synthetic aperture radar imagery, *J. Geophys. Res.*, **99**, 22,391–22,400.

Münchow, A., and E. C. Carmack, 1997: Synoptic flow and density observations neat an Arctic shelf break, *J. Phys. Oceanogr.*, **27**, 1402–1419.

Overland, J. E., and A. T. Roach, 1987: Northward flow in the Bering and Chukchi Seas, *J. Geophys. Res.*, **92**, 7097–7105.

Serreze, M. C., J. A. Maslanik, T. A. Scambos, F. Fetterer, J. Stroeve, K. Knowles, C. Fowler, S. Drobot, R. G. Barry, and T. M. Haran, 2003: A record minimum arctic sea ice extent and area in 2002, *Geophys. Res. Lett.*, **30**, 1110, doi:10.1029/2002GL016406.

Shimada, K., E. Carmack, K. Hatakeyama, and T. Takizawa, 2001: Varieties of shallow temperature maximum waters in the western Canadian basin of the Arctic Ocean, *Geophys. Res. Lett.*, **28**, 3441–3444.

Signorini, S. R., A. Münchow, and D. Hadvogel, 1997: Flow dynamics of a wide Arctic canyon, *J. Geophys. Res.*, **102**, 18,661–18,680.

Weingartner, T. J., D. J. Cavalieri, K. Aagaard, and Y. Sasaki, 1998: Circulation, dense water formation, and outflow on the northeast Chukchi shelf, *J. Geophys. Res.*, **103**, 7647–7661.